Temperature dependence of x-ray photoelectron diffraction from copper: Surface and bulk effects

R. Trehan and C. S. Fadley
Department of Chemistry, University of Hawaii at Manoa, Honolulu, Hawaii 96822
(Received 8 April 1985; revised manuscript received 1 August 1986)

The temperature dependence of x-ray photoelectron diffraction (XPD) effects in azimuthal distributions of Cu $2p_{3/2}$ and Cu $3p$ core-level intensities from a clean copper (001) surface has been measured in the range from 298 to 1010 K and for two polar angles of emission relative to the surface of $\theta=7°$ (highly surface sensitive) and $\theta=45°$ (more bulk sensitive). Measurements have been performed with typical angular resolutions of $\sim\pm4°-6°$, although some data obtained with a much higher resolution of $\sim\pm0.6°$ are also discussed. Very-high-angular-resolution azimuthal scans of Cu $2p_{3/2}$ intensity for θ values near 45° show much more fine structure and sensitivity to polar-angle variation than analogous results obtained at lower angular resolution. The diffraction-produced anisotropies as measured by $\Delta I/I_{\max}=(I_{\max}-I_{\min})/I_{\max}$ undergo a much greater relative decrease with increasing temperatures at $\theta=7°$ than at $\theta=45°$. Single-scattering cluster (SSC) calculations including Debye-Waller factors predict very well the observed diffraction patterns and their qualitative temperature dependence, as well as the variation of anisotropy with temperature at $\theta=7°$. At $\theta=45°$, theory significantly underestimates the decrease in anisotropy with temperature, probably due to multiple scattering effects occurring for emission along low-index directions with a high density of scattering atoms. Double scattering calculations were performed to estimate these effects and they are compared to experiment and the results of SSC calculations. The effective surface Debye temperatures as deduced from theory and experiment at $\theta=7°$ are 202 and 240 K for Cu $2p_{3/2}$ and Cu $3p$ emission, respectively, in good agreement with prior determinations. Finally, the Cu $2p_{3/2}$ XPD data for $\theta=7°$ gave no evidence for short-range surface melting effects on Cu(001) at temperatures up to $T/T_{\text{melting}}=0.74$.

I. INTRODUCTION

In several prior studies of core-level x-ray photoelectron diffraction (XPD) from single crystals of Cu(001),[1,2] Ni(001),[3] Ag(110),[4] LaB_6(001),[5] and $Ga_{1-x}Al_xAs$(110),[6] at ambient temperatures, it has been shown that a simple single-scattering cluster (SSC) model provides a very good description of the angular variations of photoelectron intensities associated with such substrate emission. These substrate XPD effects have also been discussed in terms of a less accurate Kikuchi-band model.[7] However, the SSC theory is more accurate in several respects[7(b)] and is easier to apply to general emission geometries such as near-grazing polar emission angles with very high surface sensitivity. Also, SSC theory is generally found to give better agreement with experiment,[7(b)] even for more bulk sensitive emission angles where some of the Kikuchi-band assumptions should be more nearly valid. SSC theory has also been used very successfully in describing XPD data from core levels of adsorbates on single crystals, thus providing surface structure information[1-3,8-10] More recently, such SSC calculations have also been found to be very useful in the analysis of normal-[11] and off-normal-[12]photoelectron diffraction data and in providing structural information on epitaxial overlayer growth.[13] Thus, although more accurate theoretical models for XPD, including, for example, curved-wave scattering instead of plane-wave scattering[12(b),14,15] and multiple scattering effects[16] have been discussed, the much greater complexity of such calculations, coupled with the previously demonstrated successes of the much simpler plane-wave SSC model, lead us to concentrate on the latter in this study.

Since thermal vibrations are present in a solid at all temperatures and they are expected to modify the diffracted intensities, it is of interest to study the temperature dependence of XPD patterns and to determine how well SSC calculations including Debye-Waller factors describe these results. Of importance here are the temperature dependences of both various features in the XPD curves and their overall diffraction-produced anisotropies as measured conveniently by $\Delta I/I_{\max}=(I_{\max}-I_{\min})/I_{\max}$.

Another point of interest in such a temperature-dependent study of XPD is to determine whether the presence of any degree of surface melting in the first 1–2 atomic layers before the onset of bulk melting is suggested; such effects have been predicted theoretically for surfaces of pure materials,[17] but no such phenomena have been observed in prior low-energy electron diffraction (LEED) experimental studies.[18] However, a very recent Rutherford backscattering study of Pb(110) claims to have observed such surface melting.[19]

In a recent preliminary study[20(a)] of the temperature dependence of azimuthal XPD from the Cu $2p_{3/2}$ core level of Cu(001), it has been shown that SSC calculations very well predicted most features in the diffraction patterns, as well as the variation of anisotropy with temperature at a polar angle relative to surface at $\theta=7°$. However, at $\theta=45°$, the theory significantly underestimated the decrease in anisotropy with temperature, probably due to

multiple scattering effects.

In this paper, a much more detailed study of the temperature dependence of azimuthal XPD is presented. This involves emission from both the Cu $2p_{3/2}$ and Cu $3p$ core levels of a clean Cu(001) surface, including measurements for Cu $2p_{3/2}$ at very high angular resolution. In addition, the results of calculations including double scattering effects are presented. Section II describes our experimental procedures. Experimental results are discussed in Sec. III. In Sec. IV we describe the single-scattering and double-scattering theoretical results and compare them with experiment, and our conclusions are summarized in Sec. V.

II. EXPERIMENT

The azimuthal dependence of Cu $2p_{3/2}$ and Cu $3p$ core-level intensities from a Cu(001) surface (with peaks at kinetic energies of 560 and 1420 eV, respectively) was studied as a function of temperature from 298 to 1010 K using monochromatized Al $K\alpha$ radiation at 1486.6 eV as an excitation source. In order to vary surface sensitivity, azimuthal scans were performed at two polar angles of emission relative to the surface of $\theta=7°$ and 45° (cf. Fig. 1). The electron mean free paths associated with these peaks are noted on this figure, together with estimates for Cu $2p_{3/2}$ of the mean depth in atomic layers from which elastically scattered electrons can be emitted. The azimuthal angle ϕ was measured relative to the [100] direction in the crystal.

The experimental system used was a Hewlett-Packard 5950A x-ray photoelectron spectrometer which has been specially modified to permit angular-dependent studies.[3,8] This system has a sample preparation chamber, a low-energy electron diffraction (LEED) unit, and a custom-built variable-temperature specimen goniometer with $\sim\pm0.3°$ precision in setting both θ and ϕ and full scanning ranges of $0°\leq\theta\leq120°$ and $0°\leq\phi\leq380°$. The rotations for both polar angle and azimuthal angle are driven by stepping motors interfaced to a dedicated HP 2100 A computer. The original Hewlett-Packard videcon detection system used in earlier studies[1,2] has been replaced by a more reliable and more linear Surface Science Laboratories resistive-anode detector (model 239). The solid angle accepted by the analyzer in its normal mode of operation has been determined by electron trajectory calculations to be a cone of half-angle $\theta_{1/2}=5.7°$ or 3.7° for Cu $2p_{3/2}$ or Cu $3p$ emission, respectively.[3,21] In order to permit much higher angular resolution studies, the system has been modified so that a glass microchannel plate can be inserted between the sample and the entry to the electron lens. The individual microchannels have a length/diameter ratio of 41, corresponding to a *maximum* angular deflection of $\pm[\tan^{-1}(\frac{1}{41})]=\pm1.4°$. However, proper integration of intensity over all emitting points on the specimen surface yields an *average* solid angle corresponding to a cone of $\theta_{1/2}=0.6°$.[22] Overall intensities are reduced about a factor of $\frac{1}{50}$ by inserting this microchannel plate, so only a few sets of data for the more intense Cu $2p_{3/2}$ peak were taken in this mode.

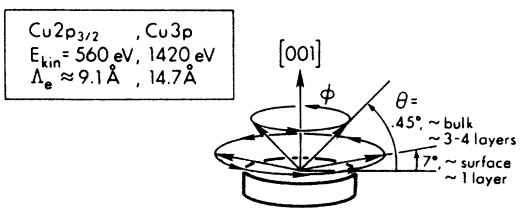

FIG. 1. Schematic illustration of the azimuthal scans carried out for a Cu(001) surface at polar angles with respect to the surface of $\theta=7°$ and 45°. The two core levels studied are Cu $2p_{3/2}$ and Cu $3p$; their kinetic energies and estimated mean free paths are indicated, as well as the mean emission depths for no-loss Cu $2p_{3/2}$ photoelectrons at the two angles studied.

The Cu single crystal was mechanically polished and oriented to within $\pm0.5°$ of (001), as judged by Laue back reflection. After final polishing with 0.05-μm Al_2O_3 abrasive, the crystal was etched with 1N HNO_3 to reduce structural disorder near the surface. Next it was aligned in the specimen goniometer by laser reflection so as to have a surface θ variation during a complete 360° rotation of less than $\pm0.3°$. Clean surfaces were prepared by Ar-ion sputtering at 400 V and 620 K and then annealing in ultrahigh vacuum at 720 K for an hour. This leads to high surface order, as verified by LEED. LEED photographs were recorded at the temperature of each azimuthal scan both prior to and after the scan to verify a stable ordered surface structure. The crystal was heated using a noninductively wound resistive button heater capable of temperatures up to ~1270 K. The complete lack of heater stray-field effects on electron angular distributions was verified by comparing high angular resolution data obtained with the heater continuously on to analogous data in which the heater current was chopped and electron counting done only during its off time. Temperatures were monitored with a thermocouple-calibrated infrared pyrometer. Surface cleanliness as monitored by XPS core-level peaks, and no detectable contaminant peaks were found after cleaning. Surface cleanliness also was checked after each azimuthal scan, and the maximum contaminant levels noted in the results reported here were 0.05 monolayers C and 0.05 monolayers O. During all measurements, base pressures in the low 10^{-10}-Torr range were maintained.

A given Cu $2p_{3/2}$ or Cu $3p$ core-level spectrum contains the peak of elastically scattered electrons together with inelastic background. The integrated elastic intensity was measured as the peak area remaining after a simple linear inelastic background subtraction.

The polar angle scale was calibrated by using a strong Cu $2p_{3/2}$ diffraction peak along the surface normal or [001] direction and the azimuthal orientation was similarly calibrated by using strong Cu $3p$ diffraction peaks along $\langle 101\rangle$ directions for emission at $\theta=45°$.[2]

All azimuthal scans, except those with high angular resolution using the microchannel plate, were carried out with ϕ steps of $\Delta\phi=4.5°$ and with full 360° rotation plus an overlap of 20° more to check instrumental stability and data reproducibility. Typical times required for these scans to achieve good statistics were $\sim2-15$ h, depending

upon the core peak and polar angle involved. Intensities are significantly higher for Cu $2p_{3/2}$ and/or for the higher polar angle of 45°. The lower-intensity Cu $2p_{3/2}$ azimuthal scans with $\theta_{1/2}=0.6°$ were performed with smaller steps of $\Delta\phi=1.8°$ and over a smaller ϕ range of 110° covering 20° more than necessary for one of the symmetry-equivalent quadrants above the (001) surface. The times required for these scans were ~17 h. because of the severe loss in intensity caused by insertion of the microchannel plate. As discussed in more detail in the following section, the diffraction features in these high-resolution azimuthal scans were *very* sensitive to slight polar angle variations, and thus very careful and accurate definition of the polar angle scale, as well as alignment of the crystal in the goniometer, were required. Polar angle calibrations via XPD peaks were thus carried out both with and without the channel plate in place. As noted previously, stray field effects from the specimen heater were verified to be negligible even with such high angle sensitivity.

A total of seven different temperatures were studied for Cu $2p_{3/2}$ emission in the range 298–1010 K,[20] as mentioned earlier. Four different temperatures were studied for Cu $3p$ emission. In addition, high angular resolution data for Cu $2p_{3/2}$ emission was obtained at three different temperatures. The Cu $2p_{3/2}$ experiments at normal angular resolution were repeated over three different Cu(001) surfaces, and good reproducibility was found with respect to all of the features of the XPD curves, their overall anisotropies, and their variation with temperature.[20]

Although temperatures above 1010 K were also studied for Cu $2p_{3/2}$ emission, these led to both a visual surface haziness and changes in the LEED patterns probably associated with (111) faceting.[20(b)] Hence, this data is not reported here. Thus, the results discussed here do not go above $T/T_{\text{melting}}=0.74$.

III. EXPERIMENTAL RESULTS

Figures 2–5 show Cu $2p_{3/2}$ and Cu $3p$ experimental azimuthal scans at $\theta=7°$ and 45° and at three different temperatures, together with curves calculated using the SSC model. In this section, we will discuss only the experimental data. The peak heights above background of various strong features relative to that of the strongest feature at a given temperature are also shown. These relative heights are clearly affected by temperature.

All experimental data shown in Figs. 2–5 have been presented as fourfold-averaged plots of a full 360-degree scan of core-level intensity versus ϕ. Such averaging reduces noise and permits checking self-consistency by comparing the average to the individual quadrants of raw data.[2,3] All experimental anisotropies $\Delta I/I_{\max}=(I_{\max}-I_{\min})/I_{\max}$ also refer to these fourfold-averaged data. The Cu(001) surface also dictates mirror symmetry about $\phi=45°$ in each of these scans. As no mirror averaging is done in treating the data, the degree of mirror symmetry found provides a good estimate of the statistical accuracy and reliability of different features. In general, it is seen to be excellent in all of the curves presented.

We also note here that the azimuthal scans at $T=298$ K shown in Figs. 2–5 have lower anisotropies by a factor of ~0.77 to ~0.56 as compared to previously reported values for this system.[2] These discrepancies are due to a nonlinearity in the Videcon multichannel detector used in these earlier measurements.[3] Also, for the Cu $2p_{3/2}$ azimuthal scan at $\theta=7°$ and $T=298$ K shown in Fig. 2, we have observed two symmetrically placed peaks around the $\phi=45°$ point, instead of one broad peak as reported in earlier data;[2] this difference, we believe, is due to a less accurate θ alignment and/or poorer surface order in the prior study.

As noted in Fig. 1, the mean free path Λ_e for Cu $2p_{3/2}$ emission is estimated to be ~9.0 Å at 560 eV,[2,23] and, since the mean depth for no-loss emission is given by $\Lambda_e\sin\theta$,[3] we expect a mean depth of ~1 atomic layer at $\theta=7°$ and ~3–4 layers at $\theta=45°$. In the same way, the mean depths of no-loss emission expected for Cu $3p$ emission with $\Lambda_e\sim15.0$ Å are ~2 layers at $\theta=7°$ and ~5–6 layers of $\theta=45°$. Thus, the 7° data for both levels are ex-

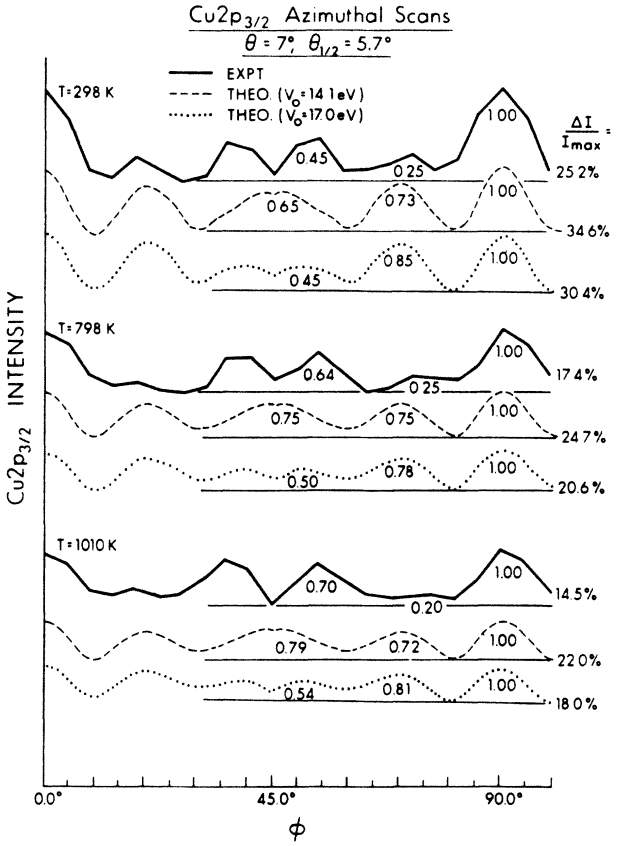

FIG. 2. Experimental and theoretical Cu $2p_{3/2}$ azimuthal scans at the very surface sensitive polar angle of $\theta=7°$ and at three different temperatures. The numbers ≤1.00 below peaks in each curve are relative peak heights as measured with respect to the maximum intensity $I_{\max}$. Overall percent anisotropies $(I_{\max}-I_{\min})/I_{\max}=\Delta I/I_{\max}$ are given at right. Two sets of theoretical curves are shown, one with an inner potential of $V_0=14.1$ eV [as taken from previous estimates (Refs. 31–33)] and another with an empirical value of 17.0 eV chosen to best fit the experimental curves. The analyzer acceptance is a cone of half-angle $\theta_{1/2}=5.7°$.

pected to be extremely surface sensitive, but that of Cu $2p_{3/2}$ somewhat more so.

Figures 6 and 7 show the temperature dependence of overall anisotropies at $\theta=7°$ and 45° for Cu $2p_{3/2}$ and Cu $3p$ emission, respectively. It is apparent that the *absolute* percentage decreases in anisotropy in Figs. 6 and 7 as temperature is increased are of the same order for both the 45° and 7° data. However, if all of these anisotropies are measured relative to the value at 298 K via

$$[\Delta I/I_{\max}(T)]/[\Delta I/I_{\max}(298\ \mathrm{K})]\ ,$$

the *relative* decreases in anisotropy show even greater differences, particularly for the most surface sensitive Cu $2p_{3/2}$ data, where the 7° results show almost twice the slope of the 45° data.[20] The only nonmonotonic variation seen in these experimental data is the slight hump for Cu $2p_{3/2}$, $\theta=45°$ at $T\approx 700$ K, which was found to be reproducible.

As expected, we observe that in all cases the anisotropies of Figs. 6 and 7 decrease with increasing temperatures. For the Cu $2p_{3/2}$ core level, the relative anisotropy,

$$[\Delta I/I_{\max}(T)]/[(\Delta I/I_{\max}(298\ \mathrm{K})]\ ,$$

at $\theta=7°$ decreases by 42.5% between ambient temperature and 1010 K (from 100% to 57.5%), while that for $\theta=45°$ shows a significantly lower 22.7% decrease over the same temperature range. For Cu $3p$ emission, the relative anisotropy at $\theta=7°$ shows a decrease of 23.7% between ambient temperature and 955 K and that at $\theta=45°$ a very similar 22.7% decrease over the same temperature range. The greatest relative decrease thus occurs for the case of Cu $2p_{3/2}$ emission at $\theta=7°$. This is qualitatively understandable in light of the fact that for grazing emission and this low kinetic energy (560 eV), we expect a mean depth of no-loss emission of only ~ 1 atomic layer. Since mean-square displacements of atoms in the top layer are expected to be about twice as high as those of bulk atoms,[24] a much greater degree of vibrational disorder exists in this layer as compared to the second and deeper layers at high temperatures. This should lead to a greater loss of anisotropy for our most surface sensitive case, and such effects are discussed more quantitatively in the following section.

Concerning the question of surface melting preceding that in the bulk,[17] if this would have occurred at some higher temperature, then a sudden decrease in anisotropy for the very surface sensitive Cu $2p_{3/2}$ emission at $\theta=7°$ might be expected, with considerable loss in structure in the XPD pattern. Clearly, nothing of this sort is observed in Fig. 2 at up to $T=1010$ K. Also, LEED patterns characteristic of the Cu(001) surface could be observed at

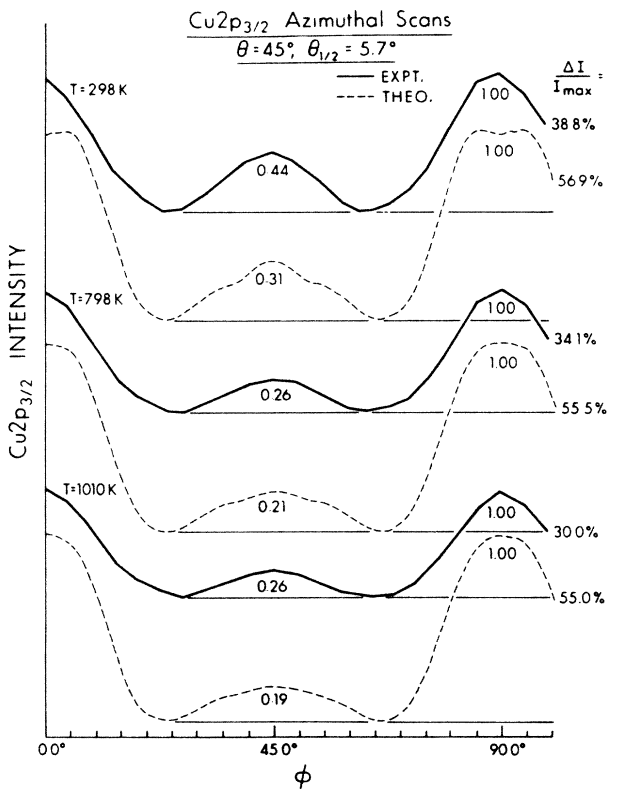

FIG. 3. The same as Fig. 2, but for a more bulk sensitive emission angle of $\theta=45°$. Here, only the unadjusted $V_0=14.1$ eV was used in the theoretical calculations.

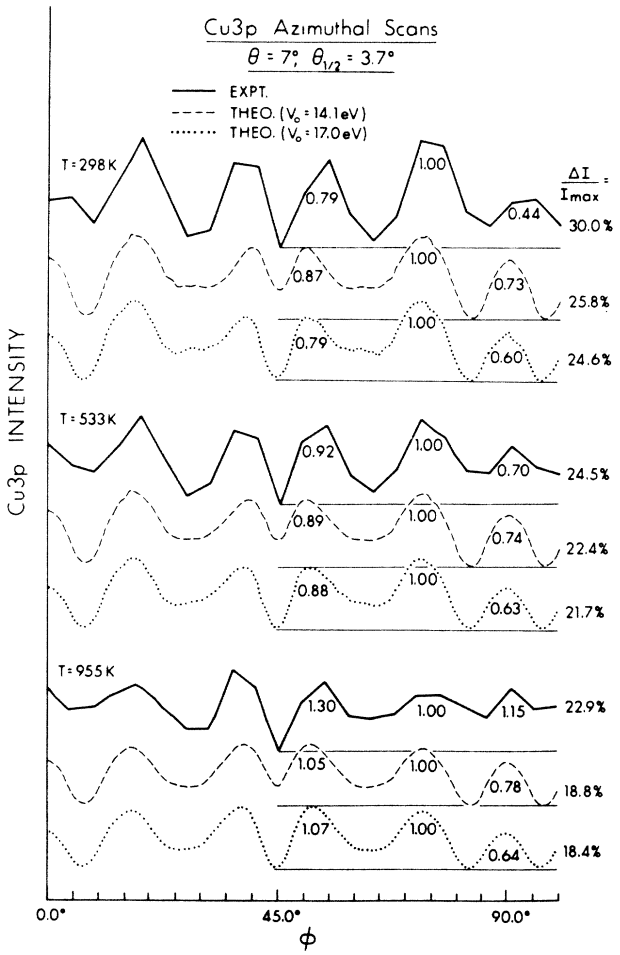

FIG. 4. The same as Fig. 2, but for Cu $3p$ emission. Again, two V_0 values have been used. The analyzer acceptance here corresponds to a half angle of 3.7°.

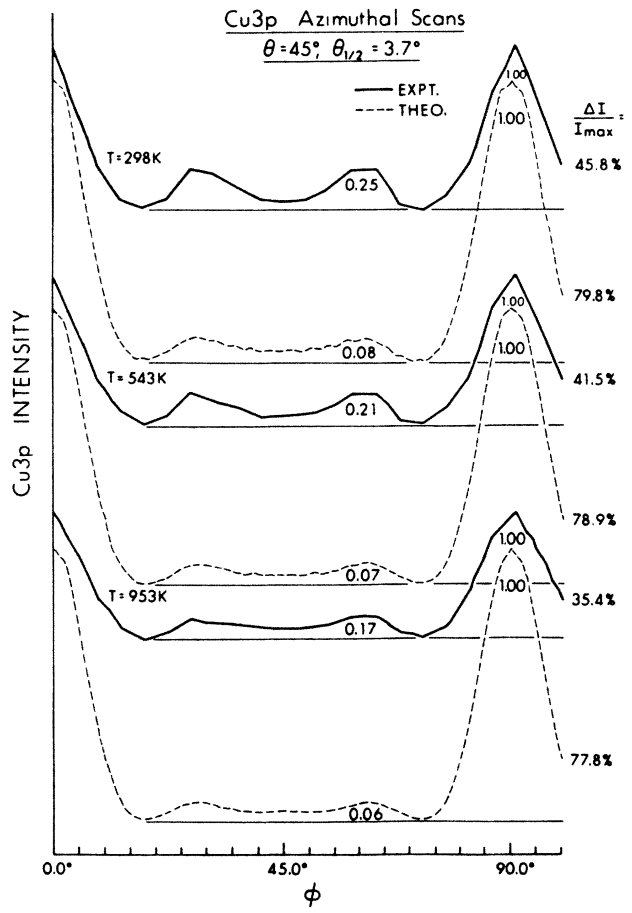

FIG. 5. The same as Fig. 3, but for Cu $3p$ emission.

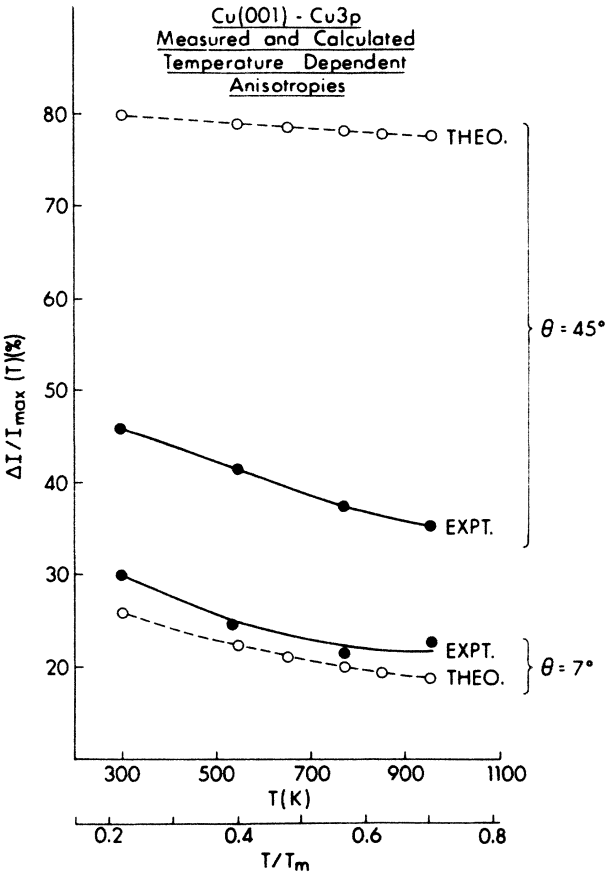

FIG. 7. The same as Fig. 6, but for Cu $3p$ emission.

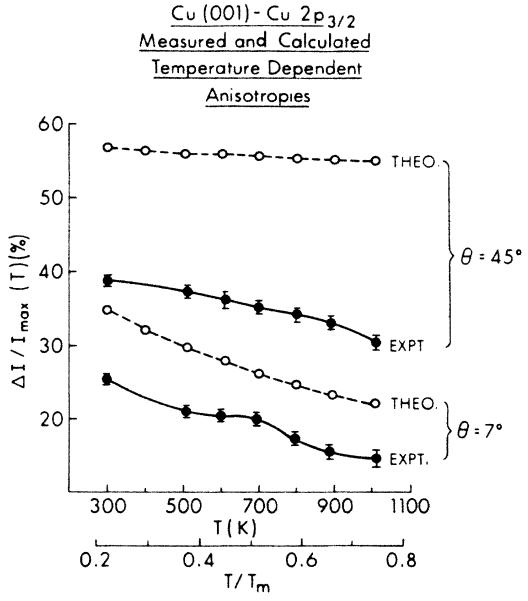

FIG. 6. Experimental and theoretical temperature-dependent anisotropies for Cu $2p_{3/2}$. Results are shown for the two polar angles of emission 45° and 7° as a function of temperature T and the ratio T/T_{melting}.

up to 1010 K. It is also noteworthy that XPD should be sensitive to very short-range order,[2,3] whereas LEED is sensitive to much larger domains of ~ 100 Å in size. Overall, these results thus point to the absence of any short-range surface premelting for Cu(001) at up to $T=1010$ K or $T/T_{\text{melting}}=0.74$.

Finally, Figs. 8 and 9 show Cu $2p_{3/2}$ data with high angular resolution. A comparison of the azimuthal scans at $\theta=45°$ in Fig. 3 and in Figs. 8 and 9 clearly shows that the high angular resolution data have a much finer structure. Features such as those labeled b, c, and d are completely absent from the data of Fig. 3 with $\theta_{1/2}=5.7°$ where we instead have only a broad single peak centered at $\phi=45°$. Such additional fine structure in high angular resolution XPD from adsorbate core levels has already been found to be useful in deducing adsorbate bonding geometries more accurately.[3,25] Referring to Fig. 8, we also observe that relative intensities of features in these azimuthal scans are very sensitive to small variations in the polar angle θ at which the ϕ scan is made. A 1° change from $\theta=45°$ in either direction causes very conspicuous changes in the overall pattern, with features b and c becoming more intense, and d less intense, as θ increases. This observation has been employed in achieving more accurate alignment of the crystal.

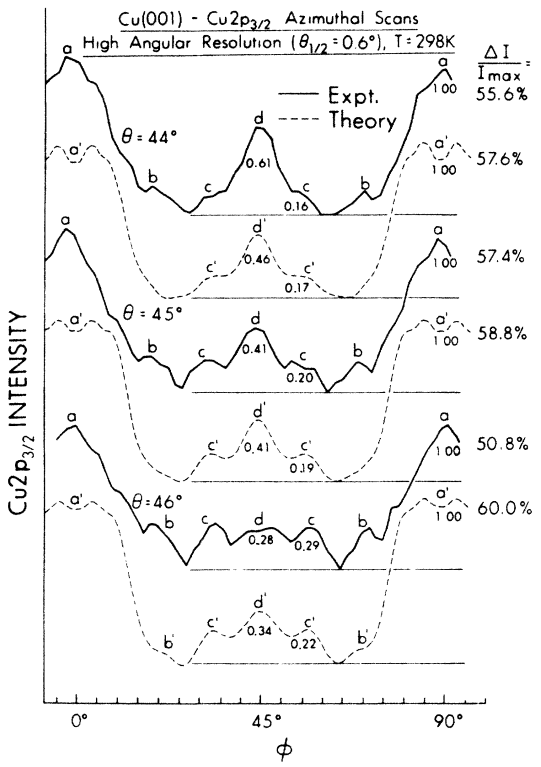

FIG. 8. Ambient-temperature experimental and theoretical Cu $2p_{3/2}$ azimuthal scans at high angular resolution with a half angle of $\theta_{1/2}=0.6°$ and at three close-spaced polar angles of emission relative to surface of $\theta=44°$, 45°, and 46°. The relative intensities of peaks *a*, *c*, and *d* above background are also indicated.

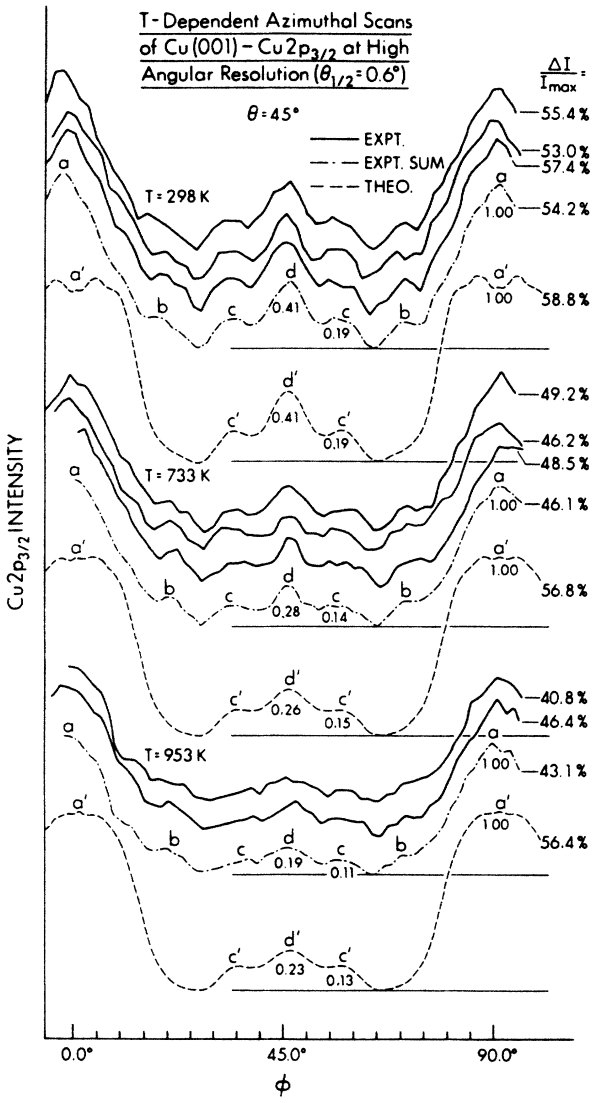

FIG. 9. Experimental and theoretical Cu $2p_{3/2}$ azimuthal scans at high angular resolution for $\theta=45°$ and at three different temperatures (298, 733, and 953 K). Again, certain relative intensities are indicated.

IV. CLUSTER DIFFRACTION CALCULATIONS AND THEIR COMPARISON WITH EXPERIMENT

A. The single-scattering cluster model

The single-scattering cluster (SSC) model used in our calculations and its various input quantities have been discussed in detail previously,[2,3,8–12] so only a brief description is given here. We consider the initial emission of a core photoelectron wave $\phi_o(\mathbf{r},\mathbf{k})$ at position $\mathbf{r}$ and with wave vector $\mathbf{k}$ from some atom in the cluster as caused by incident radiation with unit polarization vector $\hat{\varepsilon}$. The directional modulation of this photoelectron wave due to the excitation matrix element is described by either an $\hat{\varepsilon}\cdot\hat{k}$ dependence (which is exact for *s*-level emission) or, for non-*s* levels, by the more approximate square root of the differential photoelectric cross section of the core level involved.[2,3] One portion of the wave reaches the detector without scattering, whereas other portions are assumed to elastically scatter once from atoms at positions $\mathbf{r}_j$, resulting in scattered wave $\phi_j(\mathbf{r},\mathbf{k})$ that are proportional to the complex scattering factor $f_j(\theta_j)$. Before being emitted from the surface into the direction of the detector, all waves then undergo attenuation due to inelastic scattering, as well as refraction at the surface potential barrier or inner potential V_0. The intensity in a given final direction $\mathbf{k}$ is then given by

$$I(\mathbf{k}) \propto |\phi_0(\mathbf{r},\mathbf{k})+\beta\sum_j \phi_j(\mathbf{r},\mathbf{k})|^2$$
$$\propto |\phi_0^2| +\beta\phi_0\sum_j(\phi_j+\phi_j^*)+\beta^2\sum_j\sum_{j'}\phi_j\phi_{j'}^*, \quad (1)$$

where β is here introduced as an empirically useful amplitude reduction parameter[2,10] that will be discussed further in the following section.

In the scattering events, it is assumed in calculating $f_j(\theta_j)$ that the outgoing spherical wave ϕ_0 can be treated as a plane wave when it reaches a scatterer at $\mathbf{r}_j$ (the so-called small-atom approximation).[2,3,14] The attenuation

of wave *amplitudes* ϕ_0 and ϕ_j due to inelastic scattering is usually described by multiplying them by $\exp(-L/2\Lambda_e)$, where Λ_e is an electron attenuation length for *intensities*.[2,3] However, in the following section, we point out that the effective amplitude attenuation appears to be about twice as strong and much closer to $\exp(-L/\Lambda_e)$.

The effects of atomic thermal vibrations in attenuating interference effects has been included in the simplest and very standard way by multiplying each ϕ_j with a Debye-Waller factor characteristic of the scattering atom j of the form

$$W_j(T)=\exp[-\Delta k_j^2\langle U_j^2(T)\rangle] =\exp[-2k^2(1-\cos\theta_j)\langle U_j^2(T)\rangle] , \quad (2)$$

where Δk_j is the magnitude of the change in the photoelectron wave vector $\mathbf{k}$ on scattering from the jth atom of the cluster, θ_j is the corresponding scattering angle, and $\langle U_j^2(T)\rangle$ is the one-dimensional mean-squared displacement representing the motion of the jth atom with respect to the emitter. Independent motion of emitter and scatterer are implicitly assumed and $\langle U_j^2\rangle$ is taken to be isotropic.

For an unpolarized x-ray source such as that used in our experiments, an averaging over polarization vector $\hat{\varepsilon}$ is required. Assuming a simple $\hat{\varepsilon}\cdot\hat{k}$ dependence of the directional modulation of initial photoelectron wave leads to an expression for photoelectron intensity in the $\mathbf{k}$ direction as obtained by Kono *et al.*[2] and used in our calculations:

$$I(\mathbf{k})\propto |I_0+\beta\sum_j I_j W_j(T)\exp\{i[kr_j(1-\cos\theta_j)+\psi_j(\theta_j)]\}|^2+\beta^2\sum_j I_j^2[1-W_j^2(T)] , \quad (3)$$

where

$$I_0=\sin\theta_k\exp(-L/2\Lambda_e) ,$$
$$I_j=\sin\theta_{r_j}|f_j(\theta_j)|\exp(-L_j/2\Lambda_e)r_j^{-1} .$$

Also, $\psi_j(\theta_j)$ is the scattering phase shift, L is the path length for inelastic scattering from emitter to surface, and L_j is that from emitter to jth scatterer to surface. θ_k and θ_{r_j} are the angles between direction of radiation propagation and $\mathbf{k}$ and $\mathbf{r}_j$, respectively. Finally, all azimuthal XPD scans were calculated with appropriate $\mathbf{k}$ averaging over 9 points to simulate the appropriate analyzer angular acceptance.[2]

B. Choices of input parameters

The scattering factors $f_j(\theta_j)$ and their associated scattering phase shifts $\psi_j(\theta_j)$ used here are calculated in a muffin-tin potential approximation using a program due to Pendry.[26] These scattering factors were used previously in SSC calculations of the azimuthal XPD for Cu(001) at ambient temperature.[2] For the two energies considered here, the amplitude $|f(\theta_j)|$ shows the well-known strong peaking about the forward direction, with FWHM values of only $\sim 20°-30°$. As mentioned before, the primary photoelectron wave has been approximated as a plane wave when it reaches the scatterers. The inclusion of spherical wave character for the primary wave may be important, at least for nearest neighbors and/or for the higher-energy Cu $3p$ photoelectrons. Several prior calculations of different types of photoelectron diffraction curves with the inclusion of spherical-wave effects[12(b),15,27,28] do exhibit changes in fine structure and peak amplitudes relative to the simpler plane-wave model. Qualitatively, it is overall expected that at higher energies, the strength of forward peaking in the effective scattering factor will be diminished by as much as a factor of $\frac{1}{2}$ with spherical waves,[27,28] and we comment upon this later.

The *a priori* choice for the adjustable parameter β, which is intended to adjust the magnitude of all scattered waves ϕ_j or, more specifically, of all scattering amplitudes $|f_j(\theta_j)|$, in Eq. (2), would be $\beta=1.0$. However, detailed comparisons between XPD experimental curves and SSC theory in several prior studies,[2-5,10] as well as in this work, suggest that effective scattering amplitudes are reduced by a factor of $\beta\approx 0.4-0.5$. This empirical reduction has been attributed to several factors such as curved-wave corrections for near-neighbor scattering,[27,28] the influence of multiple scattering, and nonisotropic inelastic effects in scattering factors. In our case, the best agreement between theory and experiment will be seen to be for $\beta=0.5$, further confirming the values chosen in previous work.

The inelastic attenuation length Λ_e in copper is estimated to be 15.0 Å at a kinetic energy $E_{\rm kin}=1482$ eV and to scale as $(E_{\rm kin})^{1/2}$.[2,23] Thus, for Cu $2p_{3/2}$ and Cu $3p$ emission using Al $K\alpha$ radiation, the values are 9.1 Å and 14.7 Å, respectively. However, we have also found from comparisons between theory and experiment that the effective mean free paths for XPD in copper appear to be $\sim\frac{1}{2}$ of these values. This can also be viewed as implying a wave *amplitude* attenuation that is as rapid as *intensity* attenuation, and it also indicates that the features in XPD are associated predominantly with very short-range order in the first few spheres of neighbors around a given emitter. We note that in the prior study of ambient-temperature XPD of copper,[2] a full Λ_e value as given above was used in the SSC calculations and generally very good agreement with experiment was obtained. However, these calculations incorporated an extra degree of inelastic attenuation because of a minor error in the SSC computer program which effectively reduced the attenuation lengths. Thus our finding of a reduced effective Λ_e is not inconsistent with this earlier work, and none of the conclusions of this prior

study are affected. As in this earlier study,[2] the surface cutoff of inelastic scattering was arbitrarily set to be a plane at the Cu hard-sphere radius of 1.28 Å above the atomic centers in the top Cu layer. Our method of choosing β and Λ_e is discussed further below.

In calculating mean-squared displacements, $\langle U_j^2(T)\rangle$, the high-temperature limit of the Debye model is appropriate for our experiments and is given by[29] $\langle U_j^2(T)\rangle = 3\hbar^2 T/Mk_B\Theta_D^2$, where $\hbar$ is Planck's constant divided by 2π, T is the absolute temperature, M is the mass of the atom, k_B is the Boltzmann constant, and Θ_D is the Debye temperature. Cu-bulk and surface-Debye temperatures (Θ_D^B and Θ_D^S) were taken from prior determinations to be 343 and 225 K, respectively.[26,30] In all calculations reported here, the surface layer of Cu atoms in the cluster was assumed to vibrate with Θ_D^S and all other layers with Θ_D^B. Over the temperature range of 298–1010 K considered here, the $\langle U_j^2\rangle$ values thus increase by a factor of ~ 3.4, from 0.005 80 to 0.019 65 Å^2 for bulk emission; this corresponds to rms displacements of 2.9–5.4% of the Cu nearest-neighbor distance, respectively.

The effect of refraction at the surface is described by[2,3]

$$\tan\theta = (\sin^2\theta' - V_0/E_{\rm kin})^{1/2}/\cos\theta' ,$$

where θ and θ' are polar angles with respect to the surface outside of and inside of the crystal, respectively. The previously determined value of the inner potential of $V_0 = 14.1$ eV[31–33] was used in most of our calculations. However, for Cu $2p_{3/2}$ and Cu $3p$ emission at $\theta = 7°$, a slight adjustment of the inner potential to 17.0 eV improves the agreement between SSC theory and experiment, and is discussed further below.

The cluster used in our calculations was spread over $\sim 90°$ in azimuth, thus extending approximately $\pm 20°$ beyond one of the eight symmetry-equivalent 45° segments of the Cu(001) surface. Each layer contained approximately 80 atoms, and sufficient layers were included that the waves emitted by bottom-layer atoms and then scattered by top-layer atoms produce a maximum scattered intensity of $\lesssim 5\%$ of the primary intensity. This criterion has been found to insure convergence.[2] For SSC calculations with the empirically optimum parameters of $\beta = 0.5$ and $\Lambda_e = \frac{1}{2} \times 15.0\,(E_{\rm kin}/1482)^{1/2}$, the 5% cutoff for a Cu $2p_{3/2}$ emitter at 560 eV takes place at the 10th and 5th layers for $\theta = 45°$ and 7°, respectively. Similar cutoffs for Cu $3p$ emission at 1420 eV occurred at the 12th and 7th layers for $\theta = 45°$ and 7°, respectively. Intensities produced by emission from deeper layers with $< 5\%$ of the primary intensity were approximated by a geometric summation method described elsewhere.[2]

Figures 10–13 show calculated SSC azimuthal scans for Cu $2p_{3/2}$ and Cu $3p$ at $T = 298$ K with different choices of β, Λ_e, and V_0 and compare them with fourfold-averaged experimental data. All theoretical azimuthal scans have been calculated with $\Delta\phi = 1°$, but a 9-point averaging over the acceptance cone of $\theta_{1/2} = 5.7°$ has been included. First, consider the topmost cases denoted as $\beta = 1.0$ and $\Lambda_e =$ Full (i.e., those cases for which no adjustments of the input data in the SSC model have been made). Here, we observe that agreement between theory and experiment is fair, but that not all features are correctly predicted. For example, for the Cu $2p_{3/2}$ azimuthal scan at $\theta = 45°$ (Fig. 10), the experimentally observed peak at $\phi = 45°$ is reasonably well predicted but the single peaks in experiment at the symmetry-related points $\phi = 0°$, 90° appear in theory as doublets. These doublets can in fact be described as the extremities of Kikuchi bands associated with Bragg-like reflections at {200} and {111} sets of planes.[3,7,20(b),34] For Cu $2p_{3/2}$ emission at $\theta = 7°$ (Fig. 11), the symmetry related peaks at $\phi = 0°$, 90° in experiment are well predicted by unadjusted theory, but the region $20° < \phi < 70°$ shows poor agreement. Specifically, theory shows a single strong peak at $\phi = 45°$ while experimentally, we observe two peaks symmetrically placed around $\phi = 45°$. For Cu $3p$ emission involving much higher kinetic energy, we see that at $\theta = 45°$ (Fig. 12) all experimentally observed peaks are well predicted, although the weaker symmetry-related features at $\phi \approx 27°$,

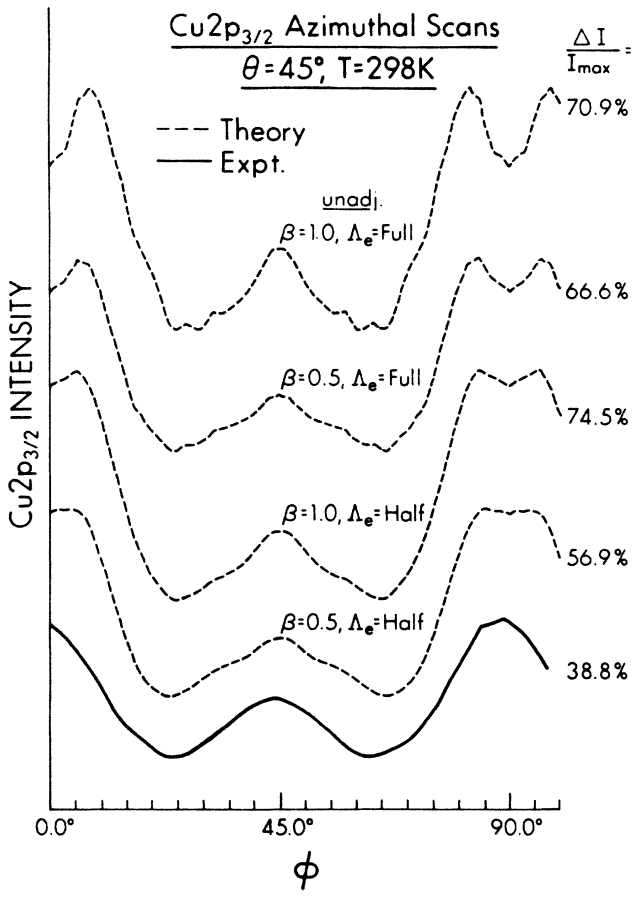

FIG. 10. Experimental and theoretical Cu $2p_{3/2}$ azimuthal scans at ambient temperature and a polar angle of 45°. The calculated curves from SSC theory have been obtained with different values of the amplitude reduction parameter β and the mean free path Λ_e. The top "unadjusted" curves correspond to the normal assumptions of the SSC model. Here, "$\Lambda_e =$ Full" refers to the value estimated from $\Lambda_e = 15.0\,(E_{\rm kin}/1482)^{1/2}$, while "$\Lambda_e =$ Half" refers to half of this value. The latter corresponds to attenuating scattered wave amplitudes as rapidly as intensities, or as $\exp(-L/\Lambda_e)$.

63° are somewhat underestimated in relative intensity and somewhat shifted in position. For Cu $3p$ emission at $\theta=7°$ (Fig. 13), the peaks at $\phi=0°$, 90° and at $\phi\approx17°$, 73°, in experiment are well predicted in unadjusted theory as to position but not relative intensity; also the features in unadjusted theory corresponding to those at $\phi\approx37°$, 53° in experiment are shifted toward one another to form an intense single peak. Moreover, unadjusted theory in all cases predicts a much higher degree of anisotropy than experiment (by factors of $\approx1.8x$ to $\approx2.4x$) and several reasons for this type of discrepancy have been discussed previously:[2,3] the presence of surface irregularities or defects not allowed for in the calculations,[2,3] spherical-wave effects in near-neighbor scattering,[3,15,28] and nonisotropic inelastic scattering.[3,35] Similar overall amplitude discrepancies between experiment and theory also are seen in x-ray absorption fine structure (EXAFS).[35–38]

Considering now the effects of selectively adjusting certain parameters, we see that reducing either scattered wave amplitudes or electron mean free paths by approximately one-half as shown in the curves marked $\beta=0.5$, $\Lambda_e=$Full, and $\beta=1.0$, $\Lambda_e=$Half causes a considerable improvement in various features. For example, for Cu $2p_{3/2}$ emission at $\theta=45°$ (Fig. 10) the valleys at $\phi=0°$, 90° become shallower . For Cu $2p_{3/2}$ emission at $\theta=7°$ (Fig. 11), the experimental peaks at $\phi\approx18°$, 72° are now almost correctly predicted in theory, although the doublet observed at $\phi=45°$ is still not predicted. Similarly, for Cu $3p$ emission at $\theta=45°$ and $\phi\approx27°$, 63° (Fig. 12), the peaks in theory now agree better in both position and relative intensity with experiment. For Cu $3p$ emission at $\theta=7°$ (Fig. 13), the minimum at $\phi=45°$ has become deeper and in much better agreement with experiment for the $\beta=0.5$, $\Lambda_e=$Full curve, and this curve also exhibits better relative peak heights. The curve marked $\beta=1.0$, $\Lambda_e=$Half shows some improvement as far as relative peak heights and anisotropy are concerned, but it does not correctly enhance the minimum observed at $\phi=45°$, particularly as compared to the curve for $\beta=0.5$, $\Lambda_e=$Full. Thus, reducing β seems most important, but reducing Λ_e also provides some improvement in agreement.

By further using the doubly adjusted combination $\beta=0.5$, $\Lambda_e=$Half, we obtain improved and generally very good agreement between theory and experiment in terms of peak positions and their approximate relative intensities for *all* of the cases in Figs. 10–13. The calculated anisotropies are also now much closer to experiment.

Finally, in order to correctly predict the minimum observed at $\phi=45°$ for Cu $2p_{3/2}$ emission at $\theta=7°$ (Fig. 11), it is found to be necessary to slightly adjust the inner potential V_0 from the generally accepted value of 14.1 (Refs. 31–33) to ~17.0 eV. Only at very low emission angles

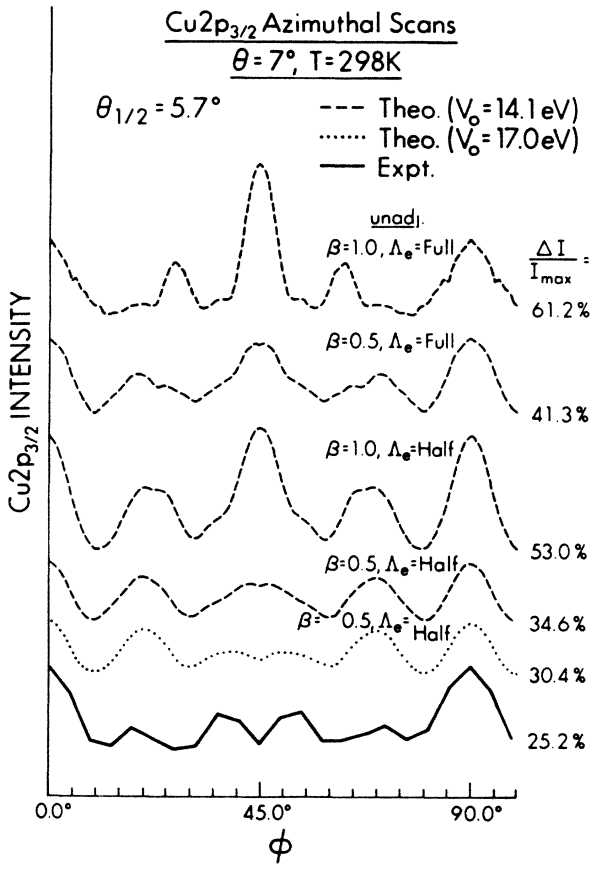

FIG. 11. The same as Fig. 10, but at a polar angle of 7°.

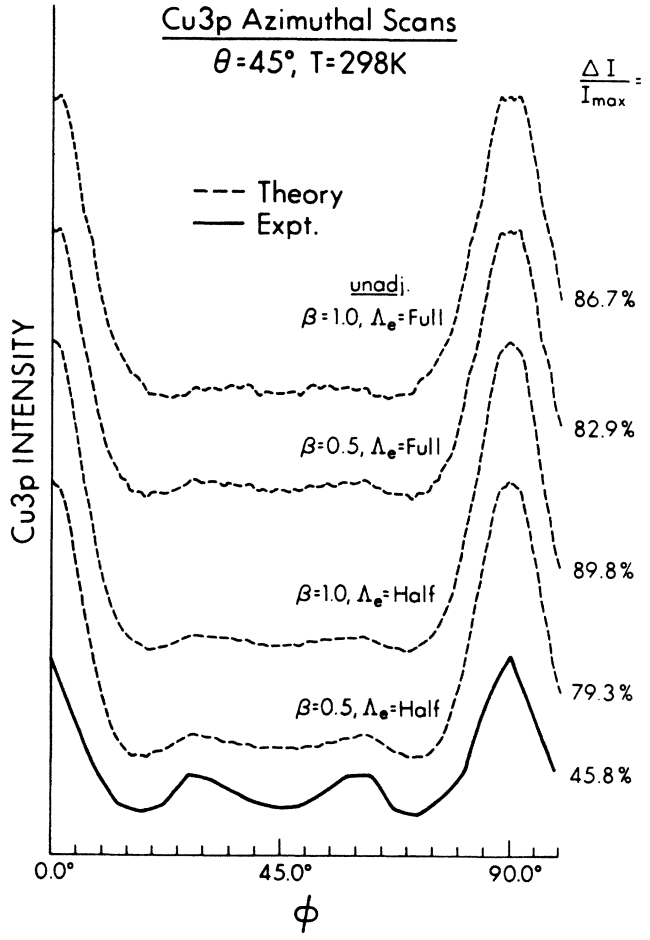

FIG. 12. The same as Fig. 10, but for Cu $3p$ emission at 45°.

are such V_0 adjustments of any consequence in XPD due to the high-electron kinetic energies involved.[3] Such an adjustment of V_0 for Cu $3p$ emission at $\theta=7°$ (Fig. 13) also improves the minimum predicted by theory at $\phi=45°$. Such empirical adjustments of V_0 are common in LEED analyses,[26] but have not been discussed previously in XPD. In the present case, the increase in effective V_0 may be associated with additional image forces acting on the photoelectron as it leaves the surface in grazing emission. These forces could have sufficient influence to deflect the photoelectron slightly toward the surface, thereby increasing the effective V_0. However, the effects of adjusting V_0 are generally rather subtle and thus all other curves reported here, as well as our analysis and conclusions, are based upon the more generally accepted value of $V_0=14.1$ eV.

In considering the results of Figs. 10–13, it is also useful to note that Eq. (1) implies that, if second-order effects in $|f_j|$ are negligible, adjusting β will not change the form of the XPD curve, but only its relative amplitude. Figures 10, 11, and 13 show the contrary: second-order effects are important.

In finally confirming our parameter choices, a large number of additional SSC calculations was performed

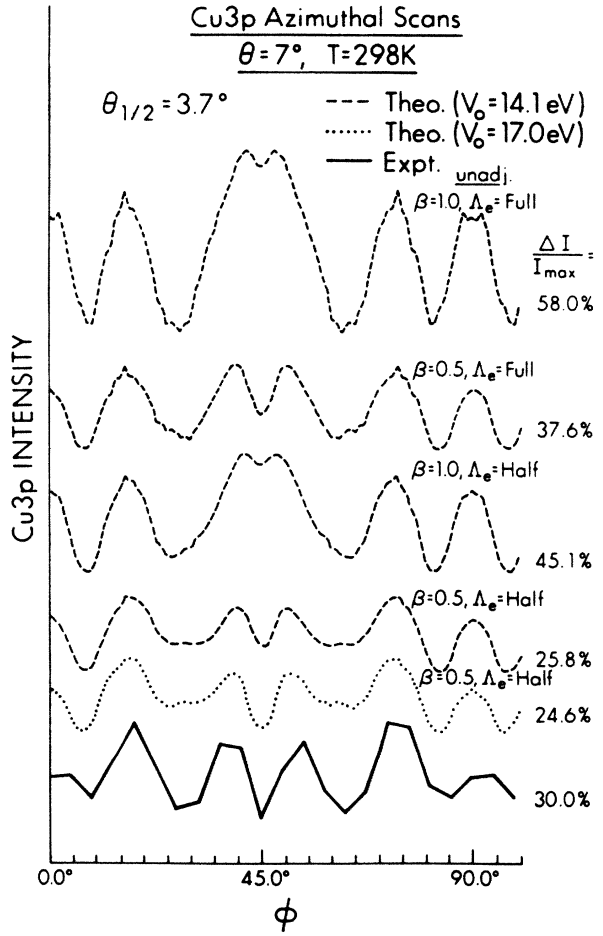

FIG. 13. The same as Fig. 12, but for a polar angle of emission of 7°.

both at $T=298$ and 1010 K and with a range of different values of β, Λ_e, and V_0. It was found that the combined use of $\beta=0.5$ and $\Lambda_e=$Half (or in some cases $\frac{3}{4}$) best describes the various features of all azimuthal XPD curves studied here, as well as their anisotropies and their temperature dependence (which will be discussed in the following section). Hence we have used the $\beta=0.5$ and $\Lambda_e=$Half combination in our analysis of the temperature-dependent XPD data. It is also worth noting here that similar reductions of scattering amplitudes via the introduction of the equivalent of our β parameter and adjustments of inelastic attenuation lengths are not unique to XPD theory, but have also been used in describing extended x-ray absorption fine structure (EXAFS) spectra.[36,37] In fact, the effective wave amplitude attenuation used in EXAFS *is* the $\exp(-L/\Lambda_e)$ that we empirically find to be best here.[37]

C. Comparison of temperature-dependent SSC calculations with experimental azimuthal data

Figures 2–5 compare the Cu $2p_{3/2}$ and Cu $3p$ experimental azimuthal scans with those calculated using SSC theory with $\beta=0.5$ and $\Lambda_e=$Half at three different temperatures. For $\theta=7°$, two choices of V_0 are also included. Considering first the Cu $2p_{3/2}$ scans, we observe that at $\theta=7°$ (Fig. 2), the agreement between theory and experiment is very good regarding peak positions and approximate relative intensities at each temperature, particularly for the curves with V_0 adjusted to 17.0 eV; the feature(s) centered at $\phi=45°$ are correctly predicted to increase in relative intensity as temperature is increased. Only the symmetry-related features at $\phi\approx20°$, 70° are consistently too intense and shifted by $\sim5°$ compared to experiment, but even here the trend of a decrease in relative intensity with increasing temperature is in general correctly predicted. For Cu $2p_{3/2}$ at $\theta=45°$ (Fig. 3) the simpler azimuthal XPD profile is well predicted at each temperature, including the decrease of relative peak intensity at $\phi=45°$ with increasing temperature.

For Cu $3p$ azimuthal scans at $\theta=7°$ and 45° (Figs. 4 and 5), agreement is excellent, with SSC theory correctly predicting all of the peak positions, their relative intensities, and the increases or decreases of these relative intensities with increasing temperature. Only the peaks for $\theta=45°$ and $\phi\approx27°$, 63° are consistently too low in intensity by $1/3x$, but their positions are very well predicted. Again, the adjustment of inner potential V_0 for Cu $3p$ emission at $\theta=7°$ is found to be advantageous in improving the agreement between theory and experiment in terms of relative peak heights and the depth of the minimum observed at $\phi=45°$. However, the adjustment of V_0 is much less important here than for the lower-energy Cu $2p_{3/2}$ case in Fig. 3. The somewhat better agreement found here for Cu $3p$ also may be due to its higher kinetic energy and a resulting lower degree of multiple scattering as compared to Cu $2p_{3/2}$.

Considering now the high angular resolution Cu $2p_{3/2}$ data at $T=298$ K and at three very closely spaced polar angles of emission (Fig. 8), we see that the agreement between SSC theory with $\beta=0.5$, $\Lambda_e=$Half and experiment

is again very good as to the prediction of fine structure and its variation with very small 1° changes in polar angle. The features *a*, *c*, and *d* are very well predicted by theory at each polar angle. Feature *b* is observed experimentally at all three θ values; in theory, it is clearly visible only in the $\theta=46°$ curve, but the trend of its increasing importance as θ increases *is* correctly predicted. Also, in going from $\theta=44°$ to 46°, the observed decrease of the relative intensity of peak *d* at $\phi=45°$ is very nicely predicted by SSC theory. One consistent discrepancy is a small minimum in the theory curves at $\phi=0°$, 90°, where a reasonably sharp peak is seen in experiment. This could be due to an enhanced importance of multiple scattering effects for emission nearly along the high-density rows of atoms belonging to the $\langle 110 \rangle$ directions and occurring for $\theta=45°$ and $\phi=0°$, 90°.

As far as the temperature dependence of such high-angular resolution Cu $2p_{3/2}$ data at $\theta=45°$ is concerned (Fig. 9), the positions and relative intensities of the observed features *a*, *c*, and *d* are well predicted by theory at all temperatures, while the weaker feature *b* is absent in theory, as noted previously. For example, the decrease of peak intensity at $\phi=45°$ with increasing temperature is very well predicted by theory.

D. Comparison of calculated and experimental anisotropies

We now consider the temperature dependence of the overall anisotropies $\Delta I/I_{\max}$ in the azimuthal scans. Figures 6 and 7 compare experimental and calculated anisotropies for Cu $2p_{3/2}$ and Cu $3p$ emission, respectively, at $\theta=7°$ and 45°. Relative anisotropies have also been calculated with normalization to the corresponding 298 K values.[20(a)] Although both experimental and theoretical curves show the same decreasing tendency with increasing temperature, several points of discrepancy are found. The most significant point is that for both Cu $2p_{3/2}$ and Cu $3p$ emission at $\theta=45°$, the calculated anisotropies are ~ 1.5–2.2 times higher than the experimental values, although, as pointed out earlier, several reasons for such discrepancies have been discussed previously.[2,3] Furthermore, it is clear that in both Cu $2p_{3/2}$ and Cu $3p$ emission at $\theta=45°$, SSC theory predicts a much slower absolute *or* relative fall of anisotropy with temperature than is observed experimentally. By contrast, the agreement between experiment and theory for both Cu $2p_{3/2}$ and Cu $3p$ at $\theta=7°$ is much better, with very similar slopes, and, for Cu $3p$, very close values of absolute anisotropies. The previously mentioned reproducible shoulder centered at ~ 700 K for Cu $2p_{3/2}$ emission at $\theta=7°$ is also absent in the theory curve (Fig. 6); this small feature is unexplained, but could be due to an onset of short-range faceting not seen in LEED or XPD. The much greater degree of disagreement in anisotropies and slopes at $\theta=45°$ could be due to enhanced multiple-scattering effects and/or our use of the plane-wave scattering approximation for near neighbors.[2,14,28] For $\theta=45°$, emission is more a multilayer phenomenon (cf. Fig. 1) and certain azimuthal angles results in electron propagation directly along rows of atoms; for example, as noted previously, $\phi=0°$, 90° is along $\langle 110 \rangle$ directions. Here, strong multiple scattering events that will be enhanced by the forward-peaked $|f_j(\theta_j)|$ with scattering angles $\theta_j \approx 0°$ are possible. By contrast, at $\theta=7°$, no such row orientations are possible, and all scattering angles must be $\geq 7°$ for this case.

Although $\Delta I/I_{\max}$ is the most reasonable measure of overall anisotropy, we should ask whether a direct comparison of experimental and theoretical $\Delta I/I_{\max}$ values can be fully quantitative, since the experimental intensity may include some fraction of essentially isotropic background I_{back} that is not allowed for in our theory. For example, emission from Cu atoms in defect sites or small disordered areas anywhere over the emitting area of the surface would tend to produce such diffuse background intensity in experimental XPD curves. (Thermal diffuse scattering would also tend to act in this way, but the SSC model attempts to allow for this.) If such effects are significant, then the experimental anisotropy can be written as

$$\begin{aligned}\Delta I/I_{\max} &= (I^{(0)}_{\max}+I_{\text{back}}-I^{(0)}_{\min}-I_{\text{back}})/(I^{(0)}_{\max}+I_{\text{back}}) \\ &= (I^{(0)}_{\max}-I^{(0)}_{\min})/(I^{(0)}_{\max}+I_{\text{back}}) ,\end{aligned}$$

where the superscript (0) indicates intensities due to emission from a perfect crystal, as assumed in theory. Thus, as noted previously, the presence of background will lower $\Delta I/I_{\max}$ relative to predictions for an ideal crystal. However, the dependence of I_{back} on temperature is very difficult to estimate, so that its effect in turn on the variation of $\Delta I/I_{\max}$ with temperature cannot be easily determined. We will thus continue to use the uncorrected experimental $\Delta I/I_{\max}$ values for comparison to experiment. This procedure has also been used in a previous study of temperature-dependent swept-energy results for normal photoelectron diffraction.[39]

In order to analyze further the variation of anisotropies with temperature it is useful to introduce a theoretically derived average or effective scattering angle $\overline{\theta_j}$ as taken over all strong scatterers in the XPD emission.[20(a)] With this, the cluster sum on j of scattered waves with different Debye-Waller factors may be replaced with an approximate temperature dependence $\Delta I/I_{\max} \propto \exp[-2k^2(1-\cos\overline{\theta_j})\langle U_j^2(T)\rangle]$. As stated previously, $\langle U_j^2(T)\rangle = 3\hbar^2 T/Mk_B\Theta_D^2 \propto T$ in the high-temperature Debye limit. Thus, if the idea of an average scattering angle is valid, plots of $\ln(\Delta I/I_{\max})$ versus T are expected to be straight lines from whose slopes $\langle U_j^2(T)\rangle$ can be derived. Figures 14 and 15 show such experimental and theoretical plots for Cu $2p_{3/2}$ and Cu $3p$ emission, with several theoretical curves whose significance will be discussed below. All of these plots *are* very nearly linear, including those for the high-angular resolution Cu $2p_{3/2}$ data shown in the upper part of Fig. 14. Least-squares slopes of all of the straight lines in Figs. 14 and 15 were derived.

Our analysis of the various slopes in these two figures proceeded in the following way: First, the slope of a *theoretical* line based upon the previously mentioned Debye temperatures of $\Theta_D^B=343$ K and $\Theta_D^S=225$ K was used to derive a $\overline{\theta_j}$ value. Then this $\overline{\theta_j}$ value was used together with the corresponding *experimental* slope to determine a single effective Debye temperature. For the much

more bulk sensitive $\theta=45°$, this effective Debye temperature is taken to represent Θ_D^B, and for the very surface sensitive $\theta=7°$, it is taken to represent Θ_D^S. These empirical Debye temperatures were then used to generate a second theoretical curve, with the ratio of Θ_D^S/Θ_D^B being taken to be $\sqrt{2}=1.41$, so that surface vibrational amplitudes are twice those in the bulk. This ratio is also very close to the ratio 343 K/225 K=1.52 of prior LEED studies on copper.[26,30] A more detailed discussion of the effects of such enhanced surface vibrational amplitudes on photoelectron diffraction appears elsewhere.[28(b)]

Considering first Cu $3p$ emission at the surface-sensitive polar angle $\theta=7°$ (Fig. 15), we see that there is very good agreement between the slope of the theory curve with $\Theta_D^B=343$ K and $\Theta_D^S=225$ K (-4.98×10^{-4} K^{-1}), and the slope of the experimental curve (-4.37×10^{-4} K^{-1}). From the *theoretical* slope and surface Debye temperature of 225 K, which should dominate for the surface sensitive polar angle of 7°, we can deduce a very reasonable value for the mean scattering angle of $\overline{\theta_j}\approx9.9°$. From this value and the *experimental* slope we further infer an effective surface Debye temperature (θ_D^S) for Cu(001) of ~240 K, which is in very good agreement with prior determinations of 220–230 K.[26,30] Furthermore, with this value of Θ_D^S and an assumed effective bulk Debye temperature of $\Theta_D^B=\sqrt{2}\times\Theta_D^S\approx340$ K in the SSC model, another curve of $\ln(\Delta I/I_{\max})$ versus T was generated; the slope of this line is (-4.87×10^{-4} K^{-1}) or somewhat closer to the experiment (-4.37×10^{-4} K^{-1}). Thus, a very self-consistent picture of these results is possible.

An identical analysis of the temperature-dependent anisotropies at $\theta=45°$ for Cu $3p$ emission is shown in the upper part of Fig. 15. Here, a bulk Debye temperature of 343 K is assumed to dominate in deriving a $\overline{\theta_j}$ value of 4.1° from theory. This smaller value of 4.1° for $\overline{\theta_j}$ at $\theta=45°$ as compared to 9.9° at $\theta=7°$ is reasonable in view of the expected importance of forward scattering events with $\theta_j\approx0°$, for example, when emission at $\theta=45°$ occurs along rows of atoms for $\phi=0°$, 90°. The dominant peaks for $\theta=45°$ and $\phi=0°$, 90° of Fig. 12 also mean that these features will strongly influence the value obtained for $\Delta I/I_{\max}$. However, the slope of the upper theory curve (-3.65×10^{-5} K^{-1}) is much smaller in magnitude than that of the experimental curve (-4.01×10^{-4} K^{-1}). Again, with $\overline{\theta_j}=4.1°$ from theory and the slope of the experimental curve, as we infer an effective bulk Debye temperature (Θ_D^B) of 104 K, a value very much lower than the expected value of around 343 K. This large discrepancy is further suggestive of the presence of strong multiple scattering effects at $\theta=45°$. With $\Theta_D^B=104$ K and $\Theta_D^S=\Theta_D^B/\sqrt{2}\approx73$ K, another $\ln(\Delta I/I_{\max})$ versus T curve was generated from the SSC model; its slope of -8.41×10^{-5} K^{-1} is now closer to experiment (-4.01×10^{-5} K^{-1}), but still much smaller in magnitude.

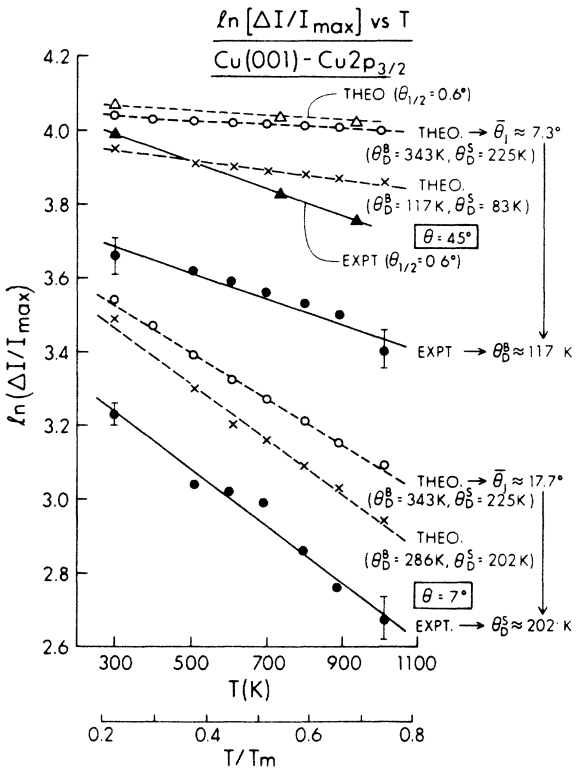

FIG. 14. The logarithm of Cu $2p_{3/2}$ azimuthal anisotropies at $\theta=45°$ and 7° are plotted as a function of temperature for experiment (●), and SSC theory (○) based upon literature values for the bulk and surface Debye temperatures. The slopes of these theory curves are used to derive an effective scattering angle $\overline{\theta_j}$, and the experimental slope is then used to derive effective bulk or surface Debye temperatures from the $\theta=45°$ or $\theta=7°$ data, respectively. The second theory curves (x) are then calculated using these empirical values of bulk (45°) and surface (7°) Debye temperatures. Also shown are values from high angular resolution experiments (▲) and a corresponding SSC theory curve (Δ) using literature bulk and surface Debye temperatures.

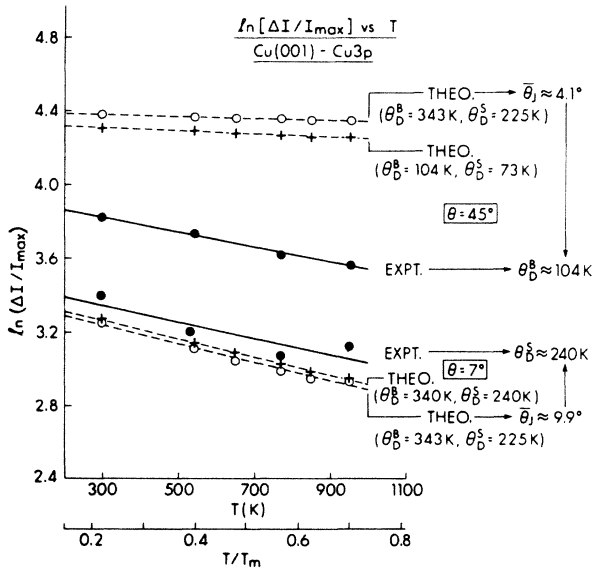

FIG. 15. The same as Fig. 14, but for Cu $3p$ emission. No high angular resolution data is reported here.

An essentially identical analysis reported previously for the Cu $2p_{3/2}$ anisotropy data[20(a)] is depicted in Fig. 14. The same conclusions were reached as were for Cu $3p$ emission. Here again at $\theta=7°$, the slope of the theory curve with $\Theta_D^B=343$ K and $\Theta_D^S=225$ K (-6.25×10^{-4} K^{-1}) and that of experiment (-7.78×10^{-4} K^{-1}) are in very good agreement, while at $\theta=45°$, the slope of the corresponding theory curve (-4.60×10^{-5} K^{-1}) is much smaller in magnitude than that of experiment (-3.44×10^{-4} K^{-1}). Using the same procedure and assumptions described above for Cu $3p$ emission, we have derived average scattering angles of $\overline{\theta_j}=17.7°$ and 7.3° for emission at polar angles of $\theta=7°$ and 45°, respectively. As for Cu $3p$ emission, the average scattering angle at $\theta=45°$ (7.3°) is much smaller than at $\theta=7°$ (17.7°), confirming the importance of strong forward scattering events with $\theta_j\approx0°$ for emission at $\theta=45°$. With these values of scattering angles and the slopes of the experimental plots at $\theta=7°$ and 45°, effective surface and bulk Debye temperatures $\Theta_D^S\sim202$ K and $\Theta_D^B\sim117$ K, respectively, were deduced. The very low value of $\Theta_D^B=117$ K is again suggestive of multiple-scattering effects at $\theta=45°$. The two values of Θ_D^S thus deduced from the Cu $2p_{3/2}$ and Cu $3p$ data (202 and 240 K) are thus consistent with one another. The lower value of $\Theta_D^S=202$ K obtained from the Cu $2p_{3/2}$ data is also reasonable in view of the fact that, for the same polar angle of emission of $\theta=7°$, the higher-energy Cu $3p$ emission occurs from somewhat deeper within the sample (cf. Fig. 1).

As for Cu $3p$, the above-deduced empirical Θ_D^S and Θ_D^B values for Cu $2p_{3/2}$ emission were then used to generate a second set of SSC curves. The slope of the second theory curve at $\theta=7°$ (-7.63×10^{-4} K^{-1}) matches almost exactly with that of experiment (-7.78×10^{-4} K^{-1}). However, at $\theta=45°$, the slope of the second theory curve with empirical Θ_D^S, Θ_D^B is -1.32×10^{-4} K^{-1}, which is somewhat closer to that of experiment (-3.44×10^{-4} K^{-1}), but still significantly smaller in magnitude.

Figure 14 also shows experimental and theoretical $\ln(\Delta I/I_{\max})$ versus T relationships for high angular resolution Cu $2p_{3/2}$ emission. The slopes of experiment and theory for these curves are -3.49×10^{-4} K^{-1} and -6.36×10^{-5} K^{-1}, respectively, and these lines are very nearly parallel to their counterparts at lower-angular resolution. Thus, the degree of angular resolution does not play a strong role in determining the temperature dependence of XPD anisotropies, although higher resolution *does* increase the absolute anisotropies by factors of $\sim1.4x$ (cf. Figs. 3 and 9).

Overall, it is thus clear that simple SSC theory with Debye-Waller factors is adequate for describing the temperature dependence of XPD anisotropies at $\theta=7°$, but for the more bulk sensitive $\theta=45°$, significant discrepancies probably due to multiple scattering emerge.

E. Effects of including double-scattering events

In order to make a first step in assessing the effect of multiple scattering on XPD temperature dependence, we have performed a series of calculations for Cu $2p_{3/2}$ emission including double scattering events. The general expression used in this work results from adding doubly scattered waves to Eq. (1) and completing the square. As discussed by Sinkovic *et al.*,[10] this yields to second order in the scattering factor products,

$$I(\mathbf{k})\propto|\phi_0|^2+\beta\phi_0\sum_j(\phi_j+\phi_j^*)+\beta'\sum_j\sum_{j'}\phi_j\phi_{j'}^* +\beta''\phi_0\sum_i\sum_j(\phi_{ij}+\phi_{ij}^*)\,, \tag{4}$$

where β is the amplitude reduction parameter discussed before, ϕ_j or $\phi_{j'}$ is a singly scattered wave proportional to a scattering amplitude $|f_j|$ or $|f_{j'}|$ as before, ϕ_{ij} is a doubly scattered wave proportional to a product of two scattering amplitudes $|f_i||f_j|$, and β' and β'' are additional amplitude reduction factors that can be adjusted in the calculations to assess the relative importance of different effects. The two double sums in Eq. (3) are thus second order in scattering amplitudes. Hence, the *a priori* scaling of β' and β'' would be $\beta'=\beta''=\beta^2$. The SSC calculations previously discussed include the first three terms of Eq. (3) and add a correction for thermal diffuse scattering[2,3] not explicitly shown above; they also implicitly use $\beta'=\beta^2$. The exact expression used for a given double scattering term ϕ_{ij} is thus [cf. Eq. (3)],

$$\phi_{ij}=\sin\theta_{r_i}\frac{|f_i(\theta_i')|}{r_i}\exp[-L_{ij}/2\Lambda_e]W_i(T)\exp\{i[kr_i(1-\cos\theta_i)+\psi_i(\theta_i')]\} \times\frac{|f_j(\theta_j')|}{|\mathbf{r}_i-\mathbf{r}_j|}W_j(T)\exp\{i[k\,|\mathbf{r}_j-\mathbf{r}_i|\,(1-\cos\theta_j')+\psi_j(\theta_j')]\}\,, \tag{5}$$

where $\mathbf{r}_i$ and $\mathbf{r}_j$ are the positions of the two scattering atoms, L_{ij} is a total path length for inelastic scattering in going from emitter to i to j to surface, θ_i is the single-scattering angle for atom i, θ_i' is the double-scattering angle from i to j and θ_j' is the double-scattering angle from j to the final detection direction $\hat{k}$. This is the same general form used previously in assessing double-scattering effects in EXAFS.[36,38] All double-scattering events were included for which the path length from emitter to i to j was $\lesssim40$ Å; this was found to yield all important events. These much more time consuming calculations were done with a ϕ step size of 4.5° and with the $\pm5.7°$ angular broadening appropriate to Cu $2p_{3/2}$.

Figure 16 shows the results of such double-scattering

(DS) calculations and compares them with corresponding SSC calculations and experiment. A comparison of the upper two curves for $\theta=45°$ shows that inclusion of double scattering events (SS + DS) at $\theta=45°$ in the unadjusted theory ($\beta=\beta'=\beta''=1.0$, $\Lambda_e=$Full) correctly tends to fill in the minimum at $\phi=0°$, 90° as compared to simple

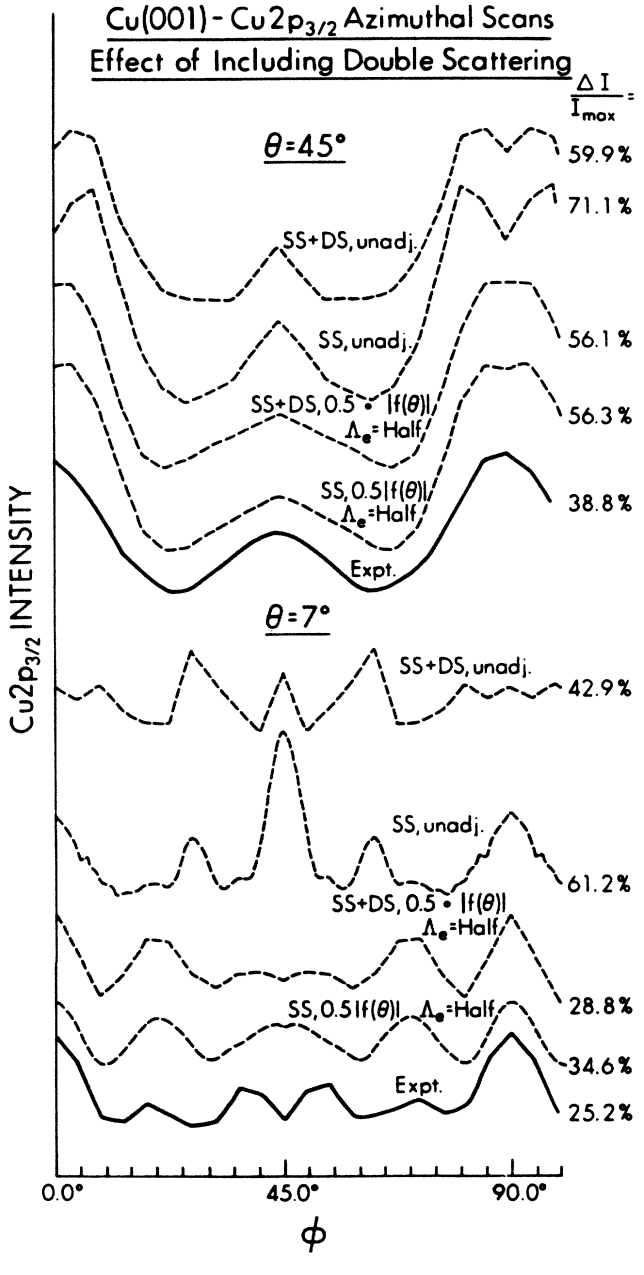

FIG. 16. Experimental and theoretical Cu $2p_{3/2}$ azimuthal scans at $T=298$ K and $\theta=45°$, 7°. The theoretical curves are calculated in four ways corresponding to single scattering only (SS) or the additional inclusion of double scattering (SS + DS), and also to whether or not the scattered wave amplitudes and Λ_e have been adjusted. The notation $0.5\,|f(\theta)|$ implies reducing all scattered-wave amplitudes to one-half of their calculated values.

SSC calculations (SS) and experiment. Including double scattering also decreases the overall anisotropy from 71.1% to 59.9% so as to be closer to experiment at 38.8%. This supports the idea that multiple scattering is important along ⟨110⟩ rows of atoms at $\phi=0°$, 90°. However, for the case of adjusted theory ($\beta=0.5$, $\beta'=\beta''=\beta^2=0.25$, and $\Lambda_e=$Half), the inclusion of double scattering for $\theta=45°$ does not significantly alter either the profile of the calculated curve or its anisotropy. The only effect of including double scattering in adjusted theory is again the filling of what is now a very minor minimum at $\phi=0°$, 90° in the corresponding SSC calculations. Furthermore, the inclusion of double scattering in adjusted theory did not improve the agreement between theory and experiment for variation of anisotropy with temperature for Cu $2p_{3/2}$ XPD at $\theta=45°$. The corresponding double scattering slope of $\ln(\Delta I/I_{\max})$ versus T is -2.80×10^{-5}, compared to -4.60×10^{-5} K^{-1} in single scattering and -3.44×10^{-4} K^{-1} in experiment. Thus, we can conclude overall that the empirical adjustment of β and Λ_e has already in large measure allowed for double scattering effects in an approximate way. However, the temperature dependence of $\Delta I/I_{\max}$ is still not adequately explained by either model at $\theta=45°$.

For Cu $2p_{3/2}$ emission at $\theta=7°$, very similar conclusions concerning double scattering effects can be made. One difference, however, is that the unadjusted double- and single-scattering curves show much greater differences than at 45°. [The previously mentioned use of β variation to determine where second-order scattering is more important is thus corroborated by these results (cf. Figs. 10 and 11).] Also, the experimentally observed minimum at $\phi=45°$ is introduced by including double scattering in the adjusted theory, even though the inner potential V_0 has been kept at the standard value of 14.1 eV (cf. Fig. 2). Thus, it may well be a concerted effect of higher V_0 and multiple scattering that produces this deep minimum in experiment.

V. CONCLUSIONS

It has been demonstrated that a simple SSC model with Debye-Waller factors and empirically reduced scattered-wave amplitudes and inelastic attenuation lengths is adequate for describing most of the features in azimuthal XPD curves for core-level emission from Cu(001) at $\theta=7°$ and 45°, even in data obtained with much higher angular resolution than prior studies. The temperature dependence of the relative intensities of different features is also in general well described by this model. With a very surface-sensitive grazing emission angle $\theta=7°$, for which multiple-scattering contributions should be reduced, overall diffraction anisotropies are also correctly predicted as a function of temperature. The usefulness of an effective scattering angle $\overline{\theta_j}$ and plots of $\ln[\Delta I/I_{\max}]$ versus T in analyzing such temperature-dependent data has also been demonstrated. Such analyses permit deriving surface Debye temperatures in good agreement with prior results. At the more bulk sensitive emission angle of $\theta=45°$, such SSC calculations very well predict the overall features of XPD curves, including the

additional fine structure observed at higher angular resolution *and* its extreme sensitivity to small variations in polar angle. However, at 45°, the temperature sensitivity of anisotropies is significantly underestimated by theory, suggesting stronger multiple scattering effects, probably along low-index rows of atoms. Such anomalously high decreases in anisotropy with temperature may be useful in future studies for identifying features with a greater influence of multiple scattering. The inclusion of double scattering in some of our calculations also points to the presence of multiple-scattering effects along rows of atoms in the crystal, and further suggests that the empirical adjustment of certain parameters in the theory allows for multiple scattering to first order. A complete description of the temperature dependence of anisotropies at $\theta=45°$ thus may require a full multiple scattering treatment. Also, the effects of including curved-wave scattering for near neighbors in such azimuthal XPD studies are worth investigating, although it is likely that our adjustment of β to ~ 0.5 also allows for this in forward scattering to a good degree.[28] Finally, no evidence of short-range surface melting was observed on Cu(001) at temperatures up to $T=1010$ K or $T/T_{\text{melting}}=0.74$.

ACKNOWLEDGMENTS

This work was supported by National Science Foundation (NSF) Grant No. CHE-83-20200.

[1]S. Kono, S. M. Goldberg, N. F. T. Hall, and C. S. Fadley, Phys. Rev. Lett. **41**, 1831 (1978).
[2]S. Kono, S. M. Goldberg, N. F. T. Hall, and C. S. Fadley, Phys. Rev. B **22**, 6085 (1980).
[3]C. S. Fadley, Prog. Surf. Sci. **16**, 275 (1984).
[4]S. Takahashi, S. Kono, H. Sakurai, and T. Sagawa, J. Phys. Soc. Jpn. **51**, 3295 (1982).
[5]S. Kono, Hyomen Kagaku (Surface Science) **2**, 153 (1981).
[6]M. Owari, M. Kudo, Y. Nihei, and H. Kamada, J. Electron. Spectrosc. Relat. Phenom. **34**, 215 (1984).
[7](a) R. J. Baird, C. S. Fadley, and L. F. Wagner, Phys. Rev. B **15**, 666 (1977); (b) S. M. Goldberg, R. J. Baird, S. Kono, N. F. T. Hall, and C. S. Fadley, J. Electron Spectrosc. Relat. Phemon. **21**, 1 (1980), and references therein.
[8]P. J. Orders, R. E. Connelly, N. F. T. Hall, and C. S. Fadley, Phys. Rev. B **24**, 6163 (1981); K. A. Thompson and C. S. Fadley, Surf. Sci. **146**, 281 (1984).
[9]P. J. Orders, B. Sinkovic, C. S. Fadley, R. Trehan, Z. Hussain, and J. Lecante, Phys. Rev. B **30**, 1838 (1984).
[10]B. Sinkovic, P. J. Orders, C. S. Fadley, R. Trehan, Z. Hussain, and J. Lecante, Phys. Rev. B **30**, 1833 (1984).
[11]P. J. Orders and C. S. Fadley, Phys. Rev. B **27**, 781 (1983).
[12](a) E. L. Bullock, C. S. Fadley, and P. J. Orders, Phys. Rev. B **28**, 4867 (1983); (b) M. Sagurton, E. L. Bullock, and C. S. Fadley, Phys. Rev. B **30**, 7332 (1984).
[13]E. L. Bullock and C. S. Fadley, Phys. Rev. B **31**, 1212 (1985).
[14]P. Lee and J. B. Pendry, Phys. Rev. B **11**, 2795 (1975).
[15]H. Takai, Y. Okumura, and A. Okiji, J. Phys. Soc. Jpn. **52**, 14 (1983).
[16]R. N. Lindsay, C. G. Kinniburgh, and J. B. Pendry, J. Electr. Spectrosc. **15**, 157 (1974).
[17]J. Q. Brougton and L. W. Woodcock, J. Phys. C **11**, 2748 (1978); E. Tosatti and L. Peitronero, Solid State Commun. **32**, 255 (1979).
[18]R. M. Goodman and G. A. Somorjai, J. Chem. Phys. **52**, 6325 (1970).
[19]J. W. M. Frenken and J. F. van der Ween, Phys. Rev. Lett. **54**, 134 (1985).
[20](a) R. Trehan, C. S. Fadley, and P. J. Orders, Solid State Commun. **50**, 315 (1984); (b) R. Trehan, Ph.D. thesis, University of Utah, 1985.
[21]R. J. Baird, Ph.D. thesis, University of Hawaii, 1977.
[22]R. C. White, C. S. Fadley, and R. Trehan, J. Electron. Spectrosc. (to be published).
[23]M. P. Seah and D. P. Dench, Surf. Int. Anal. **1**, 2 (1979).
[24]A. U. McRae, Surf. Sci. **2**, 52 (1964); S. Y. Tong, T. N. Rhodin, and A. Ignatiev, Phys. Rev. B **8**, 906 (1973); J. B. Pendry, *Low Energy Electron Diffraction* (Academic, London, 1974).
[25]R. Saiki and C. S. Fadley, XPD study of S/Ni(001) with high angular resolution (unpublished).
[26]J. B. Pendry, *Low Energy Electron Diffraction* (Academic, London, 1974), and private communication.
[27]L. G. Petersson, S. Kono, N. F. T. Hall, C. S. Fadley, and J. B. Pendry, Phys. Rev. Lett. **42**, 1545 (1979).
[28](a) M. Sagurton, E. L. Bullock, R. Saiki, A. Kaduwela, C. R. Brundle, and C. S. Fadley, Phys. Rev. B **33**, 2207 (1986); (b) M. L. Sagurton, E. L. Bullock, and C. S. Fadley, Surf. Sci. (to be published).
[29]R. W. James, *The Optical Principles of the Diffraction of X-Rays* (G. Bell and Sons, London, 1948).
[30]G. Capart, Surf. Sci. **26**, 429 (1971).
[31]L. F. Wagner, Z. Hussain, C. S. Fadley, and R. J. Baird, Solid State Commun. **21**, 453 (1977).
[32]P. Thiry, Ph.D. thesis, Université Pierre et Marie Curie, 1981.
[33]Z. Hussain, S. Kono, L. G. Petersson, C. S. Fadley, and L. F. Wagner, Phys. Rev. B **23**, 724 (1981).
[34]R. Trehan and C. S. Fadley, J. Electron. Spectrosc. (to be published).
[35]B. K. Teo and P. A. Lee, J. Am. Chem. Soc. **101**, 2815 (1979), and B. K. Teo (private communication).
[36]B. K. Teo, J. Am. Chem. Soc. **1981**, 3990 (1981).
[37]E. A. Stern, B. A. Bunker, and S. M. Heald, Phys. Rev. B **21**, 5521 (1980); E. A. Stern, D. E. Sayers, and F. W. Lytle, Phys. Rev. B **11**, 4836 (1975).
[38]A. Ashley and S. Doniach, Phys. Rev. B **11**, 1275 (1975).
[39]S. D. Kevan *et al.*, Phys. Rev. B **23**, 493 (1981).